Australian Meteorological and Oceanographic Journal 63 (2013) 249–259

Seasonal climate summary southern hemisphere (autumn 2012): The transition from La Niña to neutral

L. Martin
Tasmania and Antarctica region, Bureau of Meteorology, Australia

(Manuscript received April 2013; revised June 2013)

Southern hemisphere circulation patterns and associated anomalies for austral autumn 2012 are reviewed, with an emphasis on Pacific Basin climate indicators and Australian rainfall and temperatures. Autumn 2012 was a period of transition, with the La Niña event that had developed in spring 2011 ending in late March 2012. This was reflected by most Pacific Basin climate indicators, which shifted toward neutral values through autumn. Northern and eastern parts of Australia were wetter and cooler than normal, largely due to a very strong burst of the Madden-Julian oscillation in March and the tail end of the La Niña. In contrast, large areas of southwest Australia were much drier and warmer than usual. Tasmania was also warmer than normal, despite above average rainfall.

Introduction

This summary reviews the southern hemisphere and equatorial climate patterns for autumn 2012, with particular attention given to the Australasian and Pacific regions. The main sources of information for this report are analyses prepared by the Bureau of Meteorology's National Climate Centre and the Centre for Australian Weather and Climate Research (CAWCR).

Pacific Basin climate indices

Southern Oscillation Index

Values of the Troup Southern Oscillation Index[1] (SOI) were moderately positive in the second half of 2011, peaking in December with an SOI value of +23.0, the second-highest December SOI value on record (Webb 2012). This coincided with the peak of the 2011–12 La Niña event. From January 2012 onwards, SOI values rapidly declined as the La Niña event ended. Monthly values in autumn 2012 were neutral: +2.9 (March), –7.1 (April) and –2.7 (May), with an overall autumn average value of –2.3. Figure 1 shows the monthly SOI from January 2008 to May 2012, together with a five-month weighted moving average.

Fig. 1. Southern Oscillation Index, from January 2008 to May 2012, together with a five-month binomially weighted moving average. Means and standard deviations used in the computation of the SOI are based on the period 1933–1992.

Monthly mean sea level pressure (MSLP) was below average at both Darwin and Tahiti in March 2012, rising to above average in April and then returning to near average in May. Monthly MSLP anomalies for March, April and May for Darwin were –1.3 hPa, +1.2 hPa and +0.3 hPa respectively and at Tahiti were –0.8 hPa, +0.3 hPa and 0.0 hPa respectively. Monthly anomalies were of larger magnitude at Darwin, indicating that Darwin's MSLP had a greater influence on the SOI.

[1]The Troup Southern Oscillation Index (Troup 1965) used in this article is ten times the standardised monthly anomaly of the difference in mean-sea-level pressure (MSLP) between Tahiti and Darwin. The calculation is based on a sixty-year climatology (1933–1992). The Darwin MSLP is provided by the Bureau of Meteorology, and the Tahiti MSLP is provided by Météo France inter-regional direction for French Polynesia.

Corresponding author address: Tasmania and Antarctica Climate Services Centre, Bureau of Meteorology, GPO Box 727, Hobart Tas. 7001. l.martin@bom.gov.au.

Fig. 2. 5VAR composite standardised monthly ENSO index from January 2008 to May 2012, together with a weighted three-month moving average. See text for details.

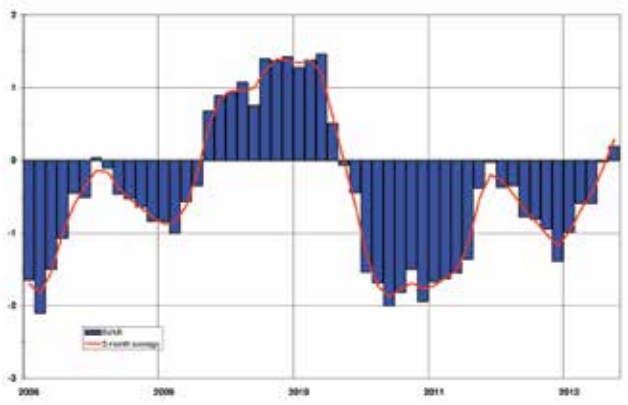

Fig. 3. OLR anomalies for autumn 2012 (W m^{-2}). Base period 1979–2000. The mapped region extends from 40°S to 40°N and from 70°E to 180°E.

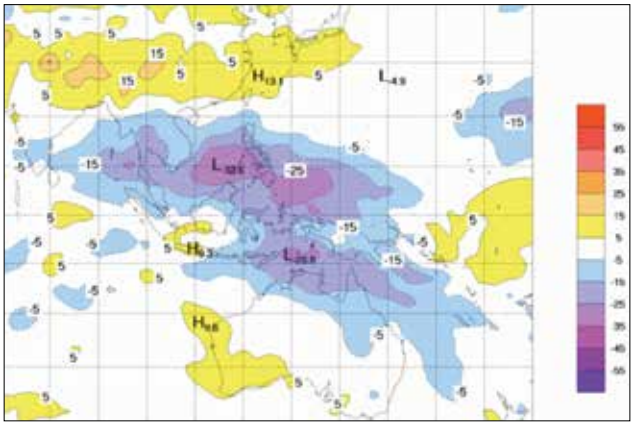

Composite monthly ENSO index 5VAR

5VAR[2] is a composite monthly ENSO index, calculated as the standardised amplitude of the first principal component of monthly Darwin and Tahiti mean sea level pressure (MSLP)[3] and monthly NINO3, NINO3.4 and NINO4 sea-surface temperatures[4] (SSTs). After a two-year period of negative 5VAR values associated with the 2010–11 and 2011–12 La Niña events (Fig. 2), 5VAR values rose through autumn 2012 as the second La Niña event ended. Monthly values of 5VAR in autumn 2012 were –0.59, –0.02 and +0.18 for March, April and May respectively, with an overall autumn average of –0.14.

The Multivariate ENSO Index[5] (MEI), produced by the U.S. Climate Diagnostics Center, is derived from a number of atmospheric and oceanic parameters calculated as a two-month mean. Large negative (positive) anomalies are usually associated with La Niña (El Niño) events. The March–April (+0.059) and April–May (+0.706) MEI values (not shown) followed an increasing trend, similar to that of the 5VAR index and consistent with neutral ENSO conditions.

Outgoing long-wave radiation

Outgoing long-wave radiation (OLR) over the equatorial Pacific Ocean is a good proxy of tropical convection, with decreases in OLR associated with increased convection and hence rainfall. During a La Niña event, OLR is often above average near the Date Line, indicating suppressed convection in that area. The opposite is true during an El Niño event. Standardised monthly anomalies[6] of OLR are computed by the Climate Prediction Center, Washington, for an equatorial region near the Date Line ranging from 5°S to 5°N and 160°E to 160°W. Monthly values for autumn 2012 were +0.8, +0.1 and –0.1 for March, April and May respectively. This indicates that convection was initially suppressed over this area, consistent with La Niña conditions, but was near-neutral in April and May when the La Niña had ended.

The spatial pattern of seasonal OLR anomalies across the Asia-Pacific tropics for autumn 2012 is shown in Fig. 3. Negative anomalies over the Maritime Continent and northern Australia were largely due to strong Madden-Julian Oscillation activity (discussed in the next section) in mid-March, as well as a burst of the north Australian monsoon. Associated rainfall totals were well above normal over large areas of northern Australia, and also over parts of central and eastern Australia. In contrast, a region of positive OLR anomalies over southern and western Western Australia was associated with well below average rainfall in those regions. Weak positive anomalies can be seen along the equator between 160°E and 180°E, consistent with the standardised anomalies discussed above.

Madden-Julian Oscillation

The Madden-Julian Oscillation (MJO) is a tropical atmospheric anomaly which develops in the Indian Ocean and propagates eastwards into the Pacific Ocean (Zhang 2005). The MJO takes approximately 30 to 60 days to reach the western Pacific, with a frequency of six to twelve events per year (Donald et al. 2004). When the MJO is in an active phase, it is associated with increased tropical rainfall, with the effects mainly concentrated during early autumn. A description of the Real-time Multivariate MJO (RMM) index and the associated phases can be found in Wheeler

[2]ENSO 5VAR was developed at the Bureau's National Climate Centre and is described in Kuleshov et al. (2009). The principal component analysis and standardisation of this ENSO index is performed over the period 1950–1999.

[3]MSLP data obtained from http://www.bom.gov.au/climate/current/soi-htm1.shtml. As previously mentioned, the Tahiti MSLP data are provided by Météo France inter-regional direction for French Polynesia.

[4]SST indices obtained from ftp://ftp.cpc.ncep.noaa.gov/wd52dg/data/indices/sstoi.indices.

[5]Multivariate ENSO Index obtained from http://www.esrl.noaa.gov/psd/people/klaus.wolter/MEI/table.html. The MEI is a standardised anomaly index described in Wolter and Timlin (1993, 1998).

[6]Standardised monthly OLR anomalies are obtained from http://www.cpc.ncep.noaa.gov/data/indices/olr

Fig. 4. Phase-space representation of the MJO index (Wheeler and Hendon 2004) for autumn 2012. Daily values are shown with March in red, April in green and May in blue. The eight MJO phases and corresponding approximate locations of the near-equatorial enhanced convective signal are labelled. Strong MJO activity is associated with daily values outside the unit circle.

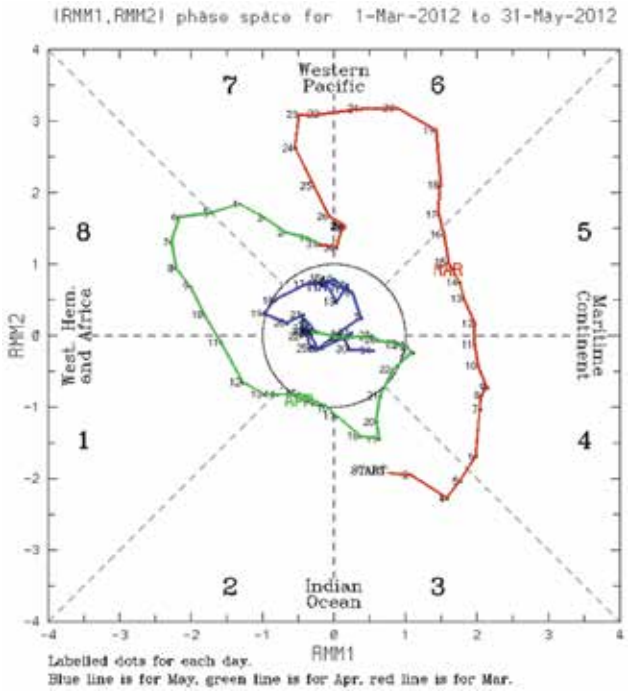

Fig. 5. Time-longitude section of daily-averaged OLR anomalies (W m^{-2}), averaged for 15°S to 15°N, for the period December 2011 through to June 2012. Anomalies are with respect to a base period of 1979–2010.

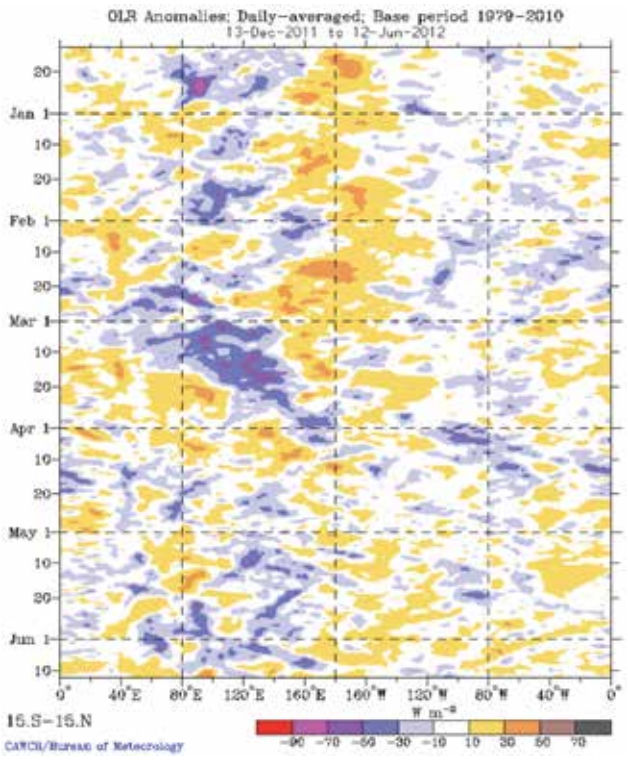

and Hendon (2004). The phase-space diagram of the RMM index for autumn 2012 is shown in Fig. 4, and the evolution of tropical convection anomalies along the equator with time shown in Fig. 5.

The MJO, which had been very strong since late January 2012, was active in the Indian Ocean (phase 3) at the start of March, moving eastwards through the Maritime Continent (phases 4 and 5) area through the middle of March. The MJO increased in strength as it progressed through the western Pacific (phase 6) between 17 and 23 March, reaching its fourth highest amplitude[7] on record for phase 6 on the 20th. The MJO weakened in phase 7, but became a bit more active as it reached the western hemisphere (phase 8), before declining in strength again after 6 April. The MJO continued to weaken as it moved through phase 1 and back into the Indian Ocean, with most points from the second half of April through May falling within the circle defined as weak MJO activity.

In Fig. 5, the negative OLR anomalies in March between 40°E and 180°E correspond with the first active burst of the MJO as it moved from the Indian Ocean, across the Maritime Continent and into the western Pacific. The second, weaker burst of the MJO can be seen in the negative OLR anomalies between 120°W and 0° in the first half of April.

[7]The amplitude of the MJO is measured by (RMM1^2 + RMM2^2)$^{1/2}$ where RMM1 and RMM2 are described by Wheeler and Hendon (2004). Records began in June 1974.

Oceanic patterns

Sea-surface temperatures

Autumn 2012 global sea surface temperature (SST) anomalies, obtained from the U.S. National Oceanic and Atmospheric Administration (NOAA) Optimum Interpolation analyses (Reynolds et al. 2002), are shown in Fig. 6. The base period is 1981–2010. Negative (cool) anomalies are shaded in blue, and positive (warm) anomalies in red.

SSTs warmed through summer 2011–12 (Webb 2012) as the La Niña weakened, conditions returning to neutral in autumn 2012. This was reflected in the pattern of SSTs in autumn, which were near normal across most of the tropical Pacific. Positive anomalies along the west coast of South America, which emerged in February, persisted through autumn. Warm anomalies were also present in the western Pacific to the north and east of Papua New Guinea, and in the central north Pacific. Residual cool anomalies remained in the central Pacific to the north of the equator, resulting from the remnants of the La Niña. SSTs were warmer than usual to the west and southeast of Australia.

All three of the standard monthly NINO indices (NINO3, 3.4 and 4) increased during autumn. In the central Pacific, the NINO3.4 index rose from –0.58 °C in March to –0.39 °C in April and –0.05 °C in May. In the eastern Pacific, NINO3 index values were –0.21 °C in March, 0.08 °C in April, and 0.15 °C in May, and in the west NINO4 values were –0.66 °C in March, –0.34 °C in April and –0.26 °C in May. Warming

Fig. 6. Anomalies of SST for autumn 2012 (°C).

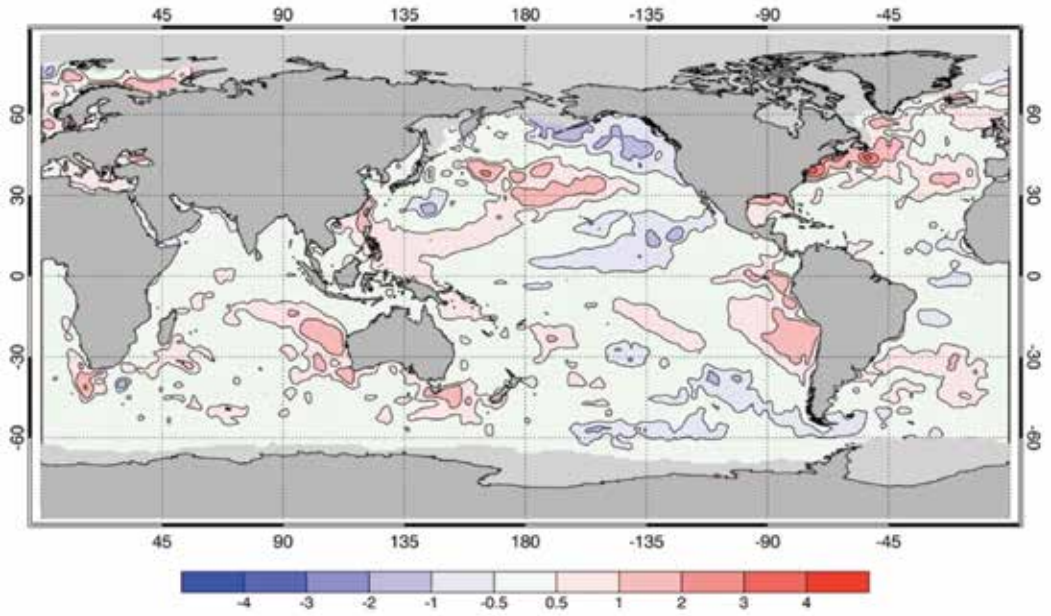

was greatest in the extreme eastern Pacific; the NINO1+2 index rose from 0.27 °C in March to 1.20 °C in May.

Subsurface patterns

The Hovmöller diagram for the 20 ºC isotherm depth anomaly along the equator from January 2009 to May 2012, obtained from NOAA's TAO/TRITON data[8], is shown in Fig. 7. The 20 ºC isotherm depth is generally located close to the equatorial thermocline, which is the region of greatest temperature gradient with depth, and is the boundary between the warm near-surface and cold deep-ocean waters. Therefore, measurements of the 20 ºC isotherm depth make a good proxy for the thermocline depth. Positive (negative) anomalies correspond to the 20 ºC isotherm being deeper (shallower) than average. Changes in the thermocline depth may act as a precursor to subsequent temperature changes at the ocean surface. A shallow thermocline depth results in more cold water available for upwelling, and therefore a potential cooling of surface temperatures.

La Niña conditions associated with the event of 2010–11, indicated by a shoaling of the thermocline in the eastern equatorial Pacific and deepening in the west, weakened slightly in autumn 2011. This was the result of a downwelling Kelvin wave which propagated eastwards across the equatorial Pacific, warming the subsurface (Tobin and Skinner 2012). La Niña conditions strengthened again in the latter half of 2011, though anomalies were weaker than in the previous summer (Webb 2012). A downwelling Kelvin wave emerged in the western Pacific in early 2012, propagating across the equatorial Pacific through autumn 2012 and bringing the La Niña event to an end, though the thermocline remained slightly deeper than usual in the

Fig. 7. Time-longitude section of the monthly anomalous depth of the 20 °C isotherm at the equator (2ºS to 2ºN) for January 2009 to May 2012. (Plot obtained from the TAO Project Office).

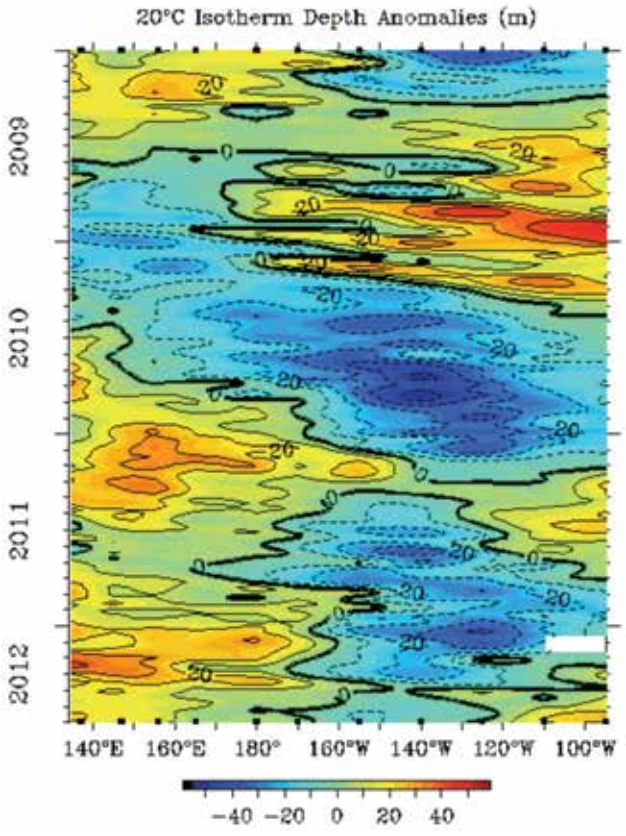

[8]Hovmöller plot obtained from http://www.pmel.noaa.gov/tao/jsdisplay/

Fig. 8. Four-month February 2012 to May 2012 sequence of vertical sea subsurface temperature anomalies at the equator for the Pacific Ocean. The contour interval is 0.5 °C. (Plot obtained from CAWCR).

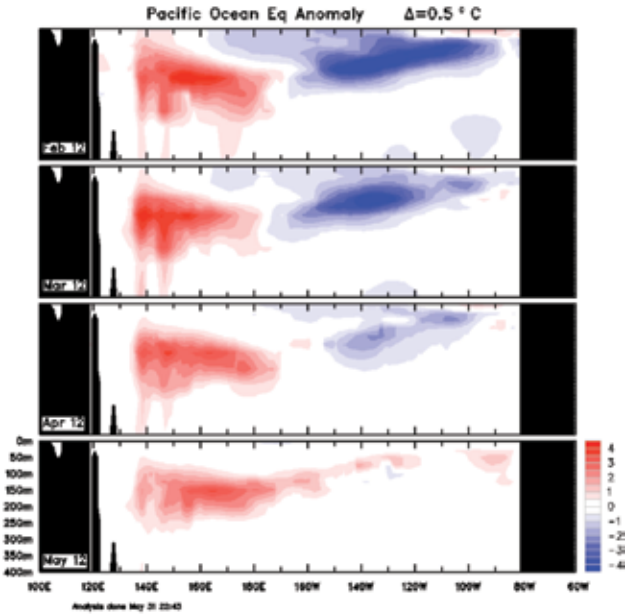

western Pacific. The decay of the La Niña in autumn 2012 is consistent with the typical life-cycle of past La Niña events.

Figure 8 shows a cross-section of monthly equatorial subsurface anomalies from February 2012 to May 2012. Red shading indicates positive (warm) anomalies, and blue shading negative (cool) anomalies. The cool sub-surface anomalies that had developed in the central and eastern Pacific during winter and spring 2011 (Cottrill 2012) started to weaken in February 2012, and continued to weaken through autumn 2012 as the La Niña event ended. Warm anomalies in the western Pacific also weakened through autumn. By May 2012 cool anomalies had almost completely disappeared from the central and eastern Pacific, with weak warm anomalies stretching from the stronger anomalies in the subsurface of the western Pacific through the central Pacific and across the top 100 m or so of the eastern Pacific Ocean, consistent with changes in the thermocline.

Atmospheric patterns

Surface analyses

The southern hemisphere autumn 2012 MSP pattern, computed using data from the 0000 UTC daily analyses of the Bureau of Meteorology's Australian Community Climate and Earth System Simulator (ACCESS) model[9], is shown in Fig. 9. The corresponding MSLP anomalies are shown in Fig. 10. Anomalies are the difference from a 1979–2000 climatology obtained from the National Centers for Environmental

[9]For more information on the Bureau of Meteorology's ACCESS model, see http://www.bom.gov.au/nwp/doc/access/NWPData.shtml

Fig. 9. Autumn 2012 MSLP (hPa). The contour interval is 5 hPa.

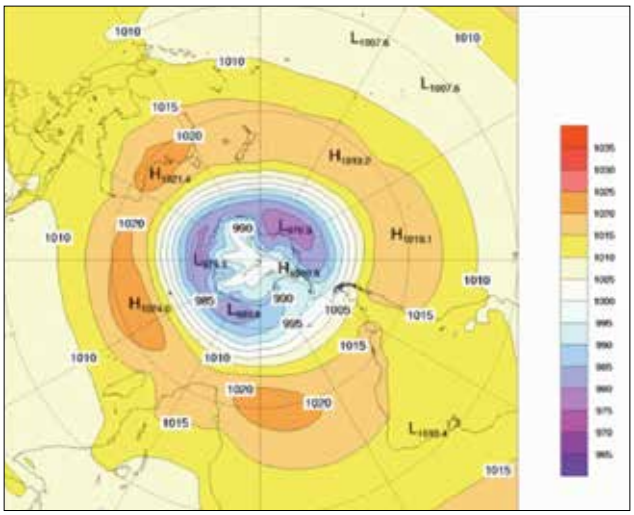

Fig. 10. Autumn 2012 MSLP anomalies (hPa), from a 1979–2000 climatology.

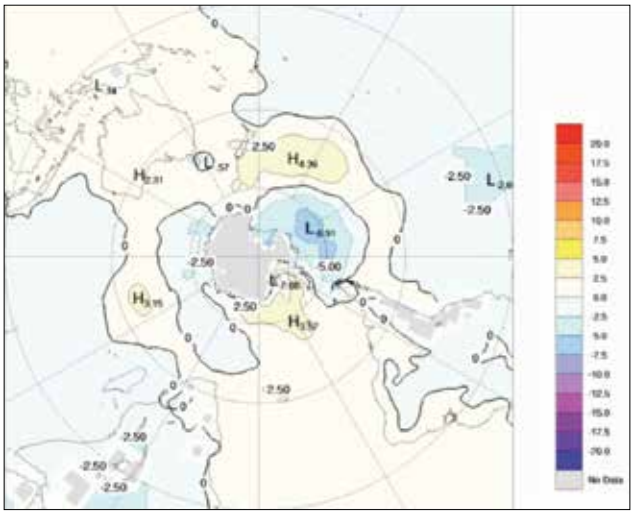

Prediction (NCEP) II Reanalysis data (Kanamitsu et al. 2002). The MSLP anomaly field is not shown over areas of elevated topography (grey shading).

The autumn MSLP pattern shows the subtropical ridge forming a band of high pressure around the southern hemisphere at about 30°S, with the main centres of high pressure located over southern Australia (1021.4 hPa), the southern Indian Ocean (1024.0 hPa), the south Atlantic (approximately 1020 hPa) and the south Pacific (1019.2 hPa and 1019.1 hPa). The circumpolar low pressure belt is evident around the Antarctic coast, with the main low pressure centres in the Amundsen Sea (976.9 hPa) and off the coast of Wilkes Land (979.3 hPa). The Antarctic high, centred over Marie Byrd Land, had a pressure of 1000.8 hPa.

MSLP was higher than normal in the Australian region, with MSLP anomalies reaching +2.3 hPa over southwest Australia. The highest MSLP anomalies were to the southeast of New Zealand, an anomaly of +4.4 hPa at about 150°W. The

strongest negative MSLP anomalies of –6.9 hPa were in the Amundsen Sea, associated with the deepest low pressure system.

Mid-tropospheric analyses

The 500 hPa geopotential height, an indicator of the steering of surface synoptic systems across the southern hemisphere, for autumn 2012 is shown in Fig. 11. The associated anomalies are shown in Fig. 12. The autumn 500 hPa height field is fairly zonal, with four weak troughs located in the Indian Ocean (~100°E), the Pacific Ocean (~180°E), near the coast of South America (~110°W) and near South Africa (~15°E). Geopotential height anomalies largely reflect MSLP anomalies (Fig. 9) south of about 40°S; positive geopotential height anomalies to the southeast of New Zealand and over Antarctica coincide with positive MSLP anomalies and negative geopotential height anomalies either side of Antarctica correspond with negative MSLP anomalies.

Fig. 11. Autumn 2012 500 hPa mean geopotential height (gpm).

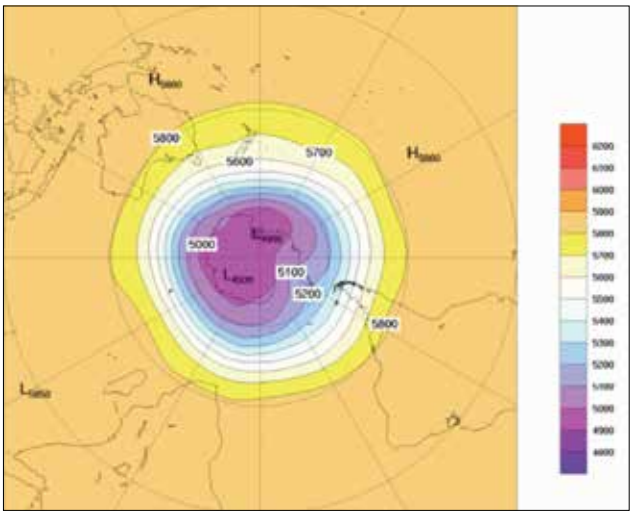

Fig. 12. Autumn 2012 500 hPa mean geopotential height anomalies (gpm), from a 1979–2000 climatology.

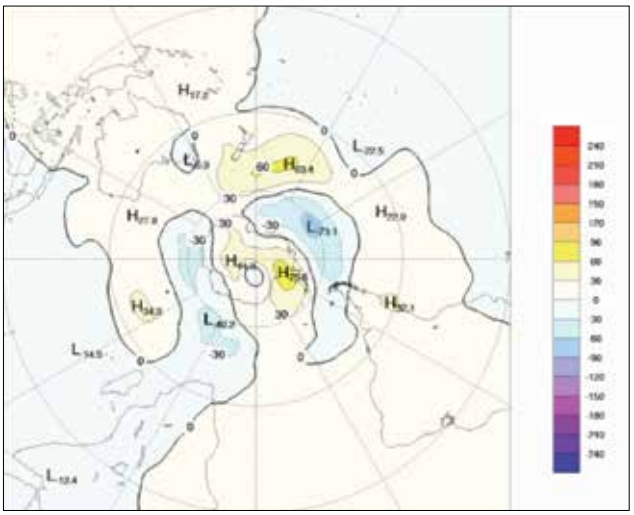

Southern Annular Mode

The Southern Annular Mode (SAM, also known as the Antarctic Oscillation or AAO) describes the oscillation of atmospheric pressure between the polar and mid-latitude regions of the southern hemisphere. Positive phases of SAM are characterised by increased mass over the extra-tropics, decreased mass over Antarctica and a poleward contraction of the mid-latitude band of westerly winds. Conversely, negative phases of SAM relate to reduced mass over the extra-tropics, increased mass over Antarctica and an equatorward expansion of the mid-latitude band of westerly winds. A similar oscillation exists in the northern hemisphere, the Northern Annular Mode, or NAM (also known as the Arctic Oscillation). The Climate Prediction Center produces a standardised monthly SAM index (Climate Prediction Center 2010)[10]. After being positive through the preceding summer, the SAM index weakened significantly but remained slightly positive through autumn 2012: +0.28 in March, +0.67 in April and +0.15 in May, resulting in a seasonal mean value of +0.36. Figures 11 and 12 show a weak high pressure anomaly over the Antarctic continent surrounded by a similarly weak ring of negative anomalies, with an area of high pressure anomalies to the south and east of New Zealand. Pressure anomalies over the Australian region were near average. The Southern Annular Mode has been shown to influence Australian rainfall and temperature patterns (Hendon et al. 2007).

Winds

Autumn 2012 low-level (850 hPa) and upper-level (200 hPa) wind anomalies (from the 22-year NCEP II climatology) are shown in Fig. 13 and 14 respectively. Isotach contours are at 5 m s^{-1} intervals. Low-level easterly winds were slightly stronger than normal (enhanced trade winds) over the western tropical Pacific Ocean, but weaker than they had been during the preceding spring and summer (Webb 2012 and Cottrill 2012), consistent with the weakening La Niña event. Weak westerly wind anomalies were also present over Indonesia and in the eastern Pacific Ocean to the north of the equator. In the upper levels, enhanced westerly wind anomalies were observed over the central Pacific Ocean to the north of the equator, associated with the enhanced Walker Circulation which weakened through autumn as the La Niña event ended.

Australian region

Rainfall

Australian rainfall totals and rainfall deciles are shown in Fig. 15 and Fig. 16 respectively. The rainfall deciles are calculated with respect to gridded rainfall data for all autumns from 1900 to 2012. A summary of seasonal rainfall ranks and

[10]For more information on the SAM index from the Climate Prediction Center (NOAA), see http://www.cpc.ncep.noaa.gov/products/precip/CWlink/daily_ao_index/aao/aao.shtml.

Fig. 13. Autumn 2012 850 hPa vector wind anomalies (m s^{-1}).

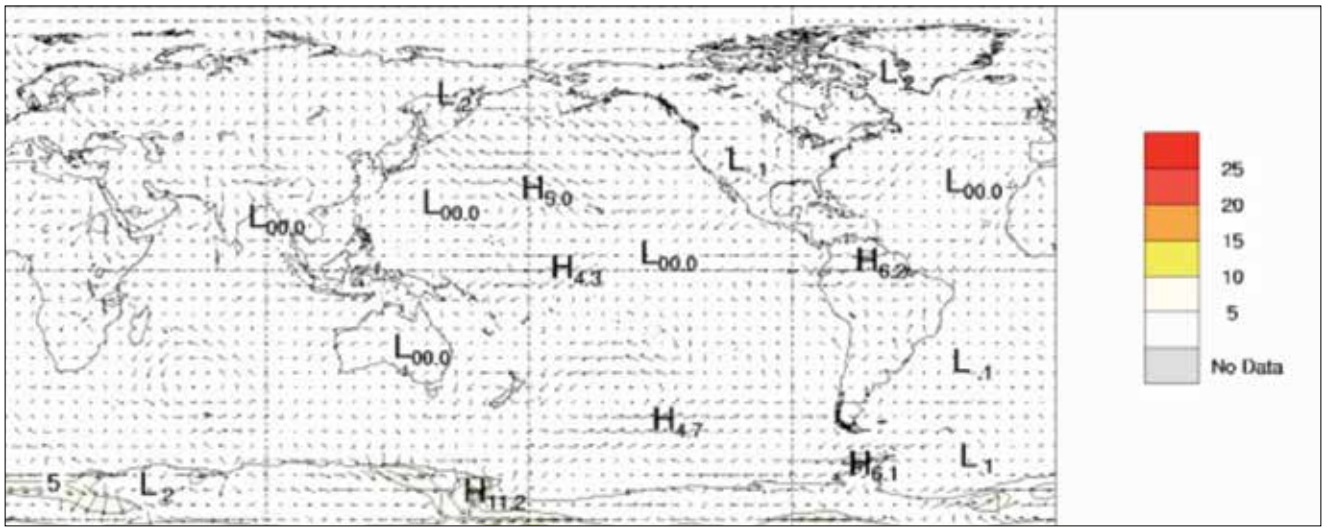

Fig. 14. Autumn 2012 200 hPa vector wind anomalies (m s^{-1}).

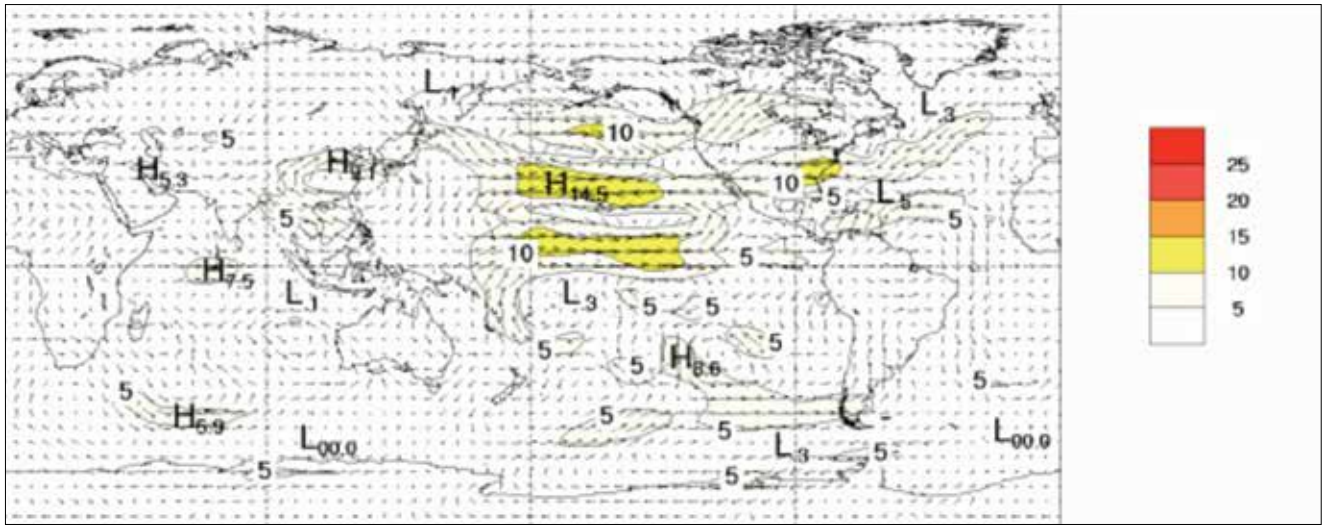

Fig. 15. Autumn 2012 rainfall totals (mm) for Australia.

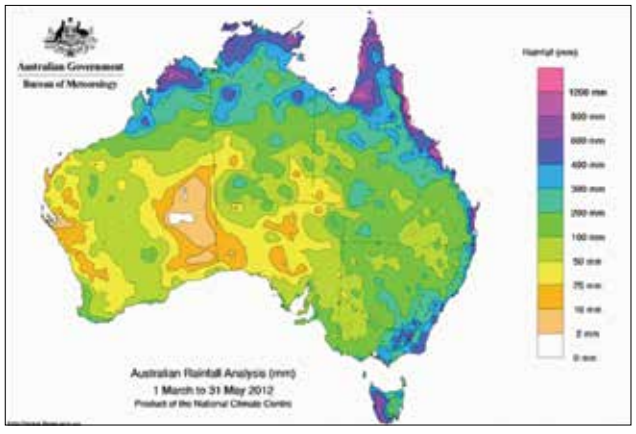

Fig. 16. Autumn 2012 rainfall deciles for Australia: decile ranges based on grid-point values over the autumns 1900–2012.

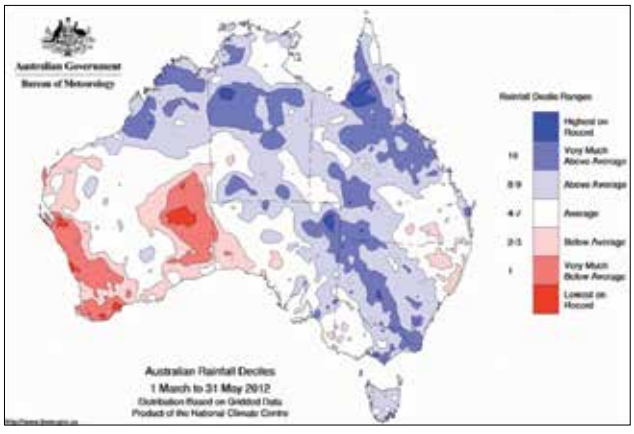

Table 1. Summary of the seasonal rainfall ranks and extremes on a national and State basis for autumn 2012. The ranking in the 2nd last column goes from 1 (lowest) to 113 (highest) and is calculated over the years 1900–2012.

Region	*Highest seasonal total (mm)*	*Lowest seasonal total (mm)*	*Highest daily total (mm)*	*Area-averaged rainfall (mm)*	*Rank of area-averaged rainfall*	*% difference from mean*
Australia	2614.8 at Bellenden Ker Bottom Station (Qld)	0.0 at Carbla Station (WA)	388.0 at Mount Jukes (Qld), 21 March	154	98	+27
Queensland	2614.8 at Bellenden Ker Bottom Station	38.0 at Durrie Station	388.0 at Mount Jukes, 21 March	244	100	+49
New South Wales	799.6 at Charlotte Pass	30.4 at Wentworth (Toora)	202.0 at Grong Grong (Berembed), 4 March	167	92	+17
Victoria	595.0 at Wyelangta	46.0 at Jeparit	166.0 at Mount Buffalo Chalet, 4 March	187	89	+19
Tasmania	1091.6 at Mount Read	114.2 at Avoca	115.2 at St Helens (Kellraine), 26 May	401	90	+18
South Australia	296.8 at Heathfield	10.2 at Oodnadatta (Allandale)	93.0 at Moomba (Tirrawarra), 3 March	55	77	–2
Western Australia	1184.0 at Home Valley	0.0 mm at Carbla Station	260.6 at Troughton Island, 14 March	91	60	0
Northern Territory	799.5 at Labelle Downs	23.0 at The Derwent	219.1 at Channel Island, 14 March	202	98	+14

Table 2. Percentage areas in different categories for autumn 2012 rainfall. 'Severe deficiency' denotes rainfall at or below the 5th percentile. Areas in decile 1 include those in 'severe deficiency', which in turn include those which are 'lowest on record'. Areas in decile 10 include those which are 'highest on record. Percentage areas of highest and lowest on record are given to two decimal places because of the small quantities involved; other percentage areas to one decimal place.

Region	*Lowest on record*	*Severe deficiency*	*Decile 1*	*Decile 10*	*Highest on record*
Australia	0.32	3.7	6.5	17.6	0.76
Queensland	0.00	0.0	0.0	30.2	2.05
New South Wales	0.00	0.0	0.0	23.2	0.16
Victoria	0.00	0.0	0.0	12.9	0.00
Tasmania	0.00	0.0	0.0	0.9	0.00
South Australia	0.00	0.0	0.9	6.0	0.55
Western Australia	0.98	11.3	19.4	7.1	0.20
Northern Territory	0.00	0.0	0.0	27.9	0.79

extremes are shown in Table 1 for each State and Territory. The percentage areas of rainfall in different categories (e.g. highest and lowest on record) are shown for each State and Territory in Table 2.

Nationally, autumn rainfall was above average (+27 per cent), the fifteenth wettest autumn of 113 years. Northern and eastern parts of Australia were the wettest: 30 per cent of Queensland observed autumn rainfall in the highest decile (wettest ten per cent of all years), 28 per cent of the Northern Territory, and 23 per cent of New South Wales. In contrast, autumn rainfall was below average over large areas of Western Australia, notably along the west coast from the Pilbara south, and in the eastern Interior and Eucla districts, although Western Australia recorded average autumn rainfall as a whole. Southwest Western Australia (southwest of a line joining Jurien Bay and Bremer Bay) had its eighth driest autumn on record. Autumn rainfall was above-average in every other State and Territory, except South Australia. Tasmania experienced its wettest autumn since 1977 with 401 mm, and Victoria its wettest autumn since 1989 with 187 mm.

The 2011–12 La Niña weakened through autumn 2012, with neutral conditions reached by the end of March. Its influence was greatest in March, when northern and eastern parts of Australia recorded their heaviest autumn rains. One of the heaviest rainfall events was due to a surface trough lingering over southeast Australia during late February and early March. Several sites in the south and west of New South Wales and northern and eastern Victoria broke autumn daily rainfall records over the first five days of March, with widespread and severe flooding on the Lachlan, Murrumbidgee, Snowy and Mitta Mitta Rivers (Bureau of Meteorology 2012). In Queensland, a tropical low pressure system produced heavy rainfall in the north and east, breaking autumn daily rainfall records between the 17th and 21st.

Fig. 17. Autumn 2012 maximum temperature anomalies (°C).

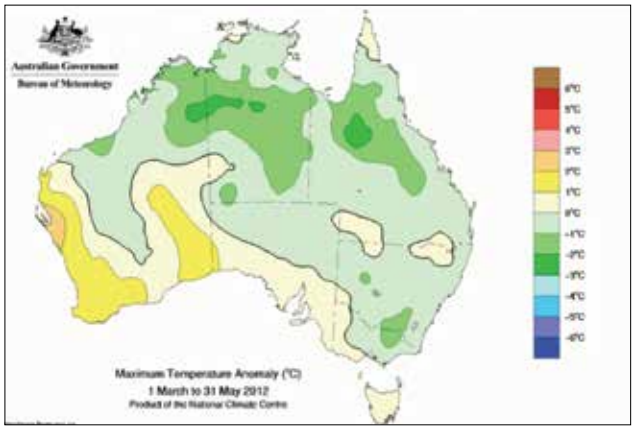

Fig. 18. Autumn 2012 maximum temperature deciles: decile ranges based on grid-point values over the autumn 1911–2012.

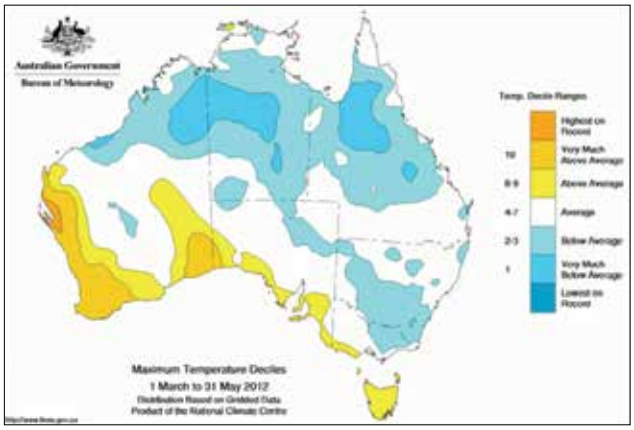

Fig. 19. Autumn 2012 minimum temperature anomalies

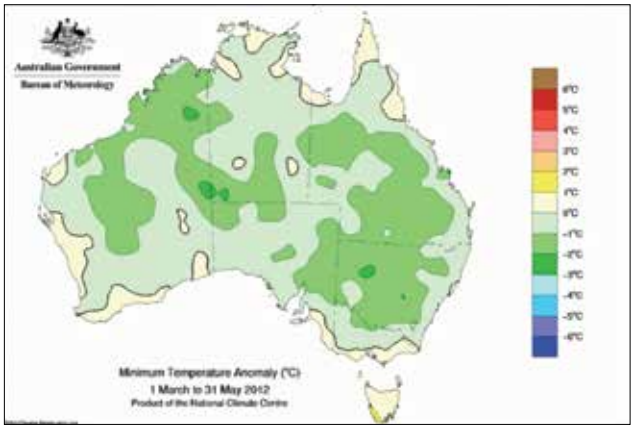

Fig. 20. Autumn 2012 minimum temperature deciles: decile ranges based on grid-point values over the autumn 1911–2012.

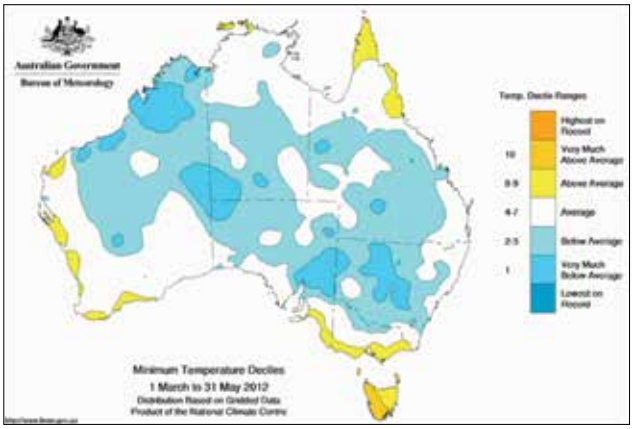

Table 3. Percentage areas in different categories for autumn 2012. Areas in decile 1 include those which are 'lowest on record'. Areas in decile 10 include those which are 'highest on record'. Percentage areas of highest and lowest on record are given to two decimal places because of the small quantities involved; other percentage areas to one decimal place. Grid-point deciles calculated with respect to 1911–2012.

Region	*Maximum temperature*				*Minimum temperature*			
	Lowest on record	*Decile 1*	*Decile 10*	*Highest on record*	*Lowest on record*	*Decile 1*	*Decile 10*	*Highest on record*
Australia	0.00	9.4	6.2	0.37	0.00	11.0	0.5	0.01
Queensland	0.00	15.0	0.0	0.00	0.00	2.4	0.0	0.00
New South Wales	0.00	0.1	0.0	0.00	0.00	23.3	0.0	0.00
Victoria	0.00	0.0	0.0	0.00	0.00	0.0	0.0	0.00
Tasmania	0.00	0.0	0.0	0.00	0.00	0.0	60.2	1.78
South Australia	0.00	0.0	2.2	0.00	0.00	16.4	0.0	0.00
Western Australia	0.00	7.4	18.2	1.14	0.00	14.2	0.0	0.00
Northern Territory	0.00	20.7	0.0	0.00	0.00	6.9	0.0	0.00

Table 4. Summary of the seasonal maximum temperature ranks and extremes on a national and State basis for autumn 2012. The ranking in the last column goes from 1 (lowest) to 103 (highest) and is calculated over the years 1910–2012[11].

Region	*Highest seasonal mean maximum (°C)*	*Lowest seasonal mean maximum (°C)*	*Highest daily temperature (°C)*	*Lowest daily maximum temperature (°C)*	*Area-averaged temperature anomaly (°C)*	*Rank of area-averaged temperature anomaly*
Australia	35.3 at Mardie (WA)	7.2 at Mount Hotham (Vic.)	44.6 at Kalbarri (WA), 9 March	–3.1 at Thredbo (Top Station) (NSW), 25 May	–0.33	36 (tied)
Queensland	32.1 at Century Mine	21.1 at Applethorpe	40.9 at Birdsville, 3 April	11.9 at Applethorpe, 25 May	–0.73	25 (tied)
New South Wales	28.0 at Mungindi	8.2 at Thredbo (Top Station)	38.2 at Tibooburra Post Office, 3 April	–3.1 at Thredbo (Top Station), 25 May	–0.40	29
Victoria	23.8 at Mildura	7.2 at Mount Hotham	35.4 at Cape Nelson, 14 March	–2.7 at Mount Hotham, 25 May	–0.13	54 (tied)
Tasmania	19.2 at Campania, Larapuna (Eddystone Point) and Launceston (Ti Tree Bend)	8.5 at Mount Wellington	30.3 at Strahan, 14 March	–1.8 at Mount Wellington, 12 May	+0.22	80
South Australia	28.3 at Marree Comparison	17.1 at Mount Lofty	40.0 at Marla, 2 April	6.3 at Mount Lofty, 24 May	+0.19	60 (tied)
Western Australia	35.3 at Mardie	22.3 at Albany	44.6 at Kalbarri, 9 March	13.5 at Rocky Gully, 31 May	+0.14	59
Northern Territory	33.9 at Bradshaw	25.8 at Arltunga	41.1 at Walungurru, 3 April	15.3 at Arltunga, 24 May	–1.12	16 (tied)

Table 5. Summary of the seasonal minimum temperature ranks and extremes on a national and State basis for autumn. The ranking in the last column goes from 1 (lowest) to 103 (highest) and is calculated over the years 1910–2012.

Region	*Highest seasonal mean minimum (°C)*	*Lowest seasonal mean minimum (°C)*	*Highest daily minimum temperature (°C)*	*Lowest daily temperature (°C)*	*Area-averaged temperature anomaly (°C)*	*Rank of area-averaged temperature anomaly*
Australia	25.9 at Troughton Island (WA)	–0.1 at Charlotte Pass (NSW)	29.0 at Varanus Island (WA), 9 March, and Onslow, 10 March (WA)	–10.0 at Charlotte Pass (NSW), 30 May	–0.80	22
Queensland	25.7 at Coconut Island	9.0 at Applethorpe	27.9 at Sweers Island, 6 March and 6 April	–3.2 at Oakey, 15 May	–0.71	37
New South Wales	17.1 at Cape Byron	–0.1 at Charlotte Pass	24.3 at Brewarrina, 1 March	–10.0 at Charlotte Pass, 30 May	–1.01	27
Victoria	13.3 at Wilsons Promontory	1.9 at Mount Hotham	21.5 at Frankston, 15 March	–0.9 at Mount Hotham Airport, 31 May	–0.23	68
Tasmania	12.7 at Swan Island	2.5 at Mount Wellington	19.7 at Flinders Island Airport, 15 March	–4.3 at Ross, 30 April	+0.72	97
South Australia	15.4 at Neptune Island	6.7 at Yongala	26.0 at Ceduna, 14 March	–3.0 at Yongala, 16 May	–0.71	25
Western Australia	25.9 at Troughton Island	8.4 at Collie East	29.0 at Varanus Island, 9 March and Onslow, 10 March	–3.4 at Wandering, 25 May	–0.77	19 (tied)
Northern Territory	25.8 at Cape Don	10.8 at Alice Springs	28.6 at Cape Don, 22 March	–2.7 at Arltunga, 17 May	–1.06	19

[11]The Australian Climate Observations Reference Network – Surface Air Temperature (ACORN-SAT) dataset (Trewin 2012) is used to calculate the spatial averages and rankings shown in Table 4 (maximum temperature) and Table 5 (minimum temperature). These averages are available from 1910 to the present.

Two tropical cyclones affected the Australian region in autumn, tropical cyclone *Koji-Joni* and severe tropical cyclone *Lua*, both in March. Tropical cyclone *Lua* formed off the northwest coast of Western Australia on 13 March, crossing the Pilbara Coast on 17 March as a category 4 cyclone and causing moderate to major flooding in the eastern Pilbara.

Drought

Prior to the autumn of 2012, widespread above-average rainfall in 2010 and 2011 had eased short-term rainfall deficiencies across Australia, including in southwest Western Australia where short-term rainfall deficiencies had persisted through January 2010 to August 2011. Below-average rainfall across parts of southern Western Australia in autumn 2012 saw rainfall deficiencies return to the southwest, with deficiencies also emerging in the southern and central interior districts.

For the three months from March to May 2012, 19 per cent of Western Australia recorded rainfall in the lowest ten per cent of records (serious deficiency), with 11 per cent of the state experiencing severe rainfall deficiencies (rainfall in the lowest five per cent of records).

Temperature

Figures 17 and 19 show the autumn 2012 maximum and minimum temperature anomalies (relative to a reference period of 1961–1990), respectively. These anomalies have been recalculated from analyses which use station normals from the 1971–2000 period, and use all stations for which an elevation is available. Station normals have been estimated using gridded climatologies for those stations with insufficient data within the 1971–2000 period, to calculate a station normal directly (see Jones et al. (2009) for more details relating to the spatial analyses of temperature data). Figures 18 and 20 show the corresponding maximum and minimum temperature deciles, calculated using monthly temperature analyses from 1911 to 2012. A summary of maximum and minimum temperature deciles for each State and Territory is shown in Table 3, with ranks and extremes in Tables 4 and 5.

Maximum temperatures averaged over Australia were 0.33 °C below normal in autumn 2012, with the largest negative anomaly recorded in the Northern Territory (–1.12 °C). While maximum temperatures were more than one degree below average across most of northern and eastern Australia, anomalies were up to two degrees above average across much of southern Western Australia, and up to one degree above average in Tasmania and southern South Australia. The highest daily maximum temperature of autumn was 44.6 °C at Kalbarri in Western Australia in March, whilst the lowest was –3.1 °C at Thredbo in New South Wales in May.

Most of Australia experienced below-average minimum temperatures in autumn 2012, except for Tasmania and some coastal fringe areas. Averaged across the country, minimum temperatures were 0.8 °C below average, the lowest since autumn 1994. The largest minimum temperature anomalies were observed in the Northern Territory (–1.06 °C) and New South Wales (–1.01 °C). The minimum temperature anomaly in Tasmania was +0.72 °C, where a few sites set new high autumn minimum temperature records. The highest minimum temperature of autumn was 29.0 °C at Varanus Island and Onslow in Western Australia in March. The lowest minimum temperature was –10.0 °C at Charlotte Pass in New South Wales in May.

References

Beard, G., Chandler, E., Watkins, A.B. and Jones, D.A. 2011. How does the 2010–11 La Niña compare with past La Niña events? *Bull. Aust. Met. Oceanogr. Soc., 24,* 17–20.

Bureau of Meteorology. 2012. Exceptionally heavy rainfall across south-east Australia. Special Climate Statement 39, Bureau of Meteorology, Melbourne.

Cottrill, A. 2012. Seasonal climate summary southern hemisphere (spring 2011): La Niña returns. *Aust. Met. Oceanogr. J., 62,* 179–92.

Donald, A., Meinke, H., Power, S., Wheeler, M. and Ribbe, J. 2004. Forecasting with the Madden-Julian Oscillation and the applications for risk management. 4th International Crop Science Congress, 26 September – 1 October 2004, Brisbane.

Hendon, H.H., Thompson, D.W.J. and Wheeler, M.C. 2007. Australian rainfall and surface temperature variations associated with the Southern Annular Mode. *J. Clim. 20,* 2452–67.

Jones, D.A., Wang, W. and Fawcett, R.J. 2009. High-quality spatial climate datasets for Australia. *Aust. Met. Oceanogr. J., 58,* 233–48.

Kanamitsu, M., Ebisuzaki, W., Woollen, J., Yang, S.-K, Hnilo, J.J., Fiorino, M. and Potter, G.L. 2002. NCEP-DOE AMIP-II Reanalysis (R-2). *Bull. Am. Meteorol. Soc., 83,* 1631–43.

Kuleshov, Y. Qi, L., Fawcett, R., and Jones, D. 2009. 'Improving preparedness to natural hazards: Tropical cyclone prediction for the southern hemisphere,' in: Gan, J. (Ed.), *Advances in Geosciences, Vol. 12 Ocean Science,* World Scientific Publishing, Singapore, 127–43.

Reynolds, R.W., Rayner, N.A., Smith, T.M., Stokes, D.C. and Wang, W. 2002. An improved in situ and satellite SST analysis for climate. *J. Clim., 15,* 1609–25.

Tobin, S. and Skinner, T.C.L. 2012. Seasonal climate summary southern hemisphere (autumn 2011): one of the strongest La Niña events on record begins to decline. *Aust. Met. Oceanogr. J., 62,* 39–50.

Trewin, B.C. 2012. Techniques involved in developing the Australian Climate Observations Reference Network – Surface Air Temperature (ACORN-SAT) dataset. CAWCR Technical Report No. 49.

Troup, A.J. 1965. The Southern Oscillation. *Q. J. R. Meteorol. Soc., 91,* 490–506.

Webb, M. 2012. Seasonal climate summary southern hemisphere (summer 2011–12): a mature La Niña, strongly positive SAM and active MJO. *Aust. Met. Oceanogr. J., 62,* 335–49.

Wheeler, M.C. and Hendon, H.H. 2004. An all-season real-time multivariate MJO Index: Development of an index for monitoring and prediction. *Mon. Weath. Rev., 132,* 1917–32.

Wolter, K. and Timlin, M.S. 1993. Monitoring ENSO in COADS with a seasonally adjusted principal component index. Proc. Of the 17th Climate Diagnostics Workshop, Norman, OK, NOAA/NMC/CAC, NSSL, Oklahoma Clim. Survey, CIMMS and the School of Meteorology, Univ. of Oklahoma, 52–7.

Wolter, K. and Timlin, M.S. 1998. Measuring the strength of ENSO – how does 1997/98 rank? *Weather, 53,* 315–24.

Zhang, C. 2005. Madden-Julian Oscillation. *Rev. Geophys., 43,* RG2003, doi: 10.1029/2004RG000158.